Post-Flight Aerodynamics Assessment of the Artemis-I Booster Separation Event

Michael W. Lee*
NASA Langley Research Center, Hampton, VA

Derek J. Dalle†, Jamie G. Meeroff‡, Stuart E. Rogers†, and Aaron C. Burkhead§
NASA Ames Research Center, Moffett Field, CA

D. Guy Schauerhamer¶ and Joshua F. Diaz¶
Science & Technology Corp., Moffett Field, CA

Rekesh Ali‖
JSEG/McLaurin Aerospace, Huntsville, AL

Peter McDonough** and Carole J. Addona††
JSEG/Jacobs, Huntsville, AL

The successful launch of the Artemis-I mission in November 2022 was made possible, in part, by years of rigorous vehicle simulation and scaled testing. Correctly anticipating the complex physics of the booster separation event was one of many necessary challenges. The successful booster separation of Artemis-I yielded flight data with which the fidelity of these predictions could be assessed. In this paper, the flight data and flight simulations are reconciled to present a unified assessment of the booster separation event. With this assessment, predictive confidence can be reinforced in support of the crewed Artemis-II mission.

Nomenclature

C_P	=	pressure coefficient
$\hat{e}_{1,2,3}$	=	unit vectors defining one axis of a local coordinate system
$\vec{p}_{01}$	=	position vector of point 1 relative to point 0
u	=	constant position vector between two points on a rigid body, in the $\hat{e}_1$ axis
v	=	constant position vector between two points on a rigid body, in the $\hat{e}_2$ axis
w	=	constant position vector between two points on a rigid body, in the $\hat{e}_3$ axis
ΔX	=	preseparation core-relative booster nose distance in the core stage x-axis
ΔY	=	preseparation core-relative booster nose distance in the core stage y-axis
ΔZ	=	preseparation core-relative booster nose distance in the core stage z-axis
BET	=	Best Estimated Trajectory
BSM	=	Booster Separation Motor
DFI	=	Developmental Flight Instrumentation
GNC	=	Guidance, Navigation, and Control
LSRB	=	Left Solid Rocket Booster
MET	=	Mission-elapsed Time

*Research Aerospace Engineer, Configuration Aerodynamics Branch, NASA Langley Research Center, AIAA Member.
†Research Aerospace Engineer, Computational Aerosciences Branch, NASA Ames Research Center
‡Supervisory Aerospace Engineer, Computational Aerosciences Branch, NASA Ames Research Center
§Intern Aerospace Engineer, Computational Aerosciences Branch, NASA Ames Research Center
¶Research Aerospace Engineer, Computational Aerosciences Branch, Science & Technology Corp.
‖Modeling and Simulation Engineer, EV42 Guidance, Navigation, and Mission Analysis Branch, JSEG/McLaurin Aerospace
**Liftoff/Separation Technical Lead, EV42 Guidance, Navigation, and Mission Analysis Branch, JSEG/Jacobs
††Booster Separation Analyst, EV42 Guidance, Navigation, and Mission Analysis Branch, JSEG/Jacobs

PMBT = Propellant Mean Bulk Temperature
RSRB = Right Solid Rocket Booster
SLS = Space Launch System
SRB = Solid Rocket Booster
TPS = Thermal Protection System

I. Background and Motivation

The Space Launch System (SLS) launched for the first time as part of the Artemis I mission on November 16, 2022 (Figure 1). The success of the first launch of this new vehicle is testament to a decade of effort across several NASA centers and contractors. Although the vehicle behavior was nominal throughout the flight, its preflight conditioning was not. Just six days prior to the successful launch, the vehicle sat on the launch pad while Tropical Storm Nicole blew through the launch complex. Prior to their integration into the final launch vehicle, the core stage RS-25 engines underwent two full burn tests at NASA Stennis Space Center, after individual engine tests had already been conducted. The consistent performance of the SLS through these planned and unplanned stress tests was only possible because of the rigor with which the vehicle was designed. Indeed, the launch vehicle fidelity is derived from the vehicle design and analysis fidelity.

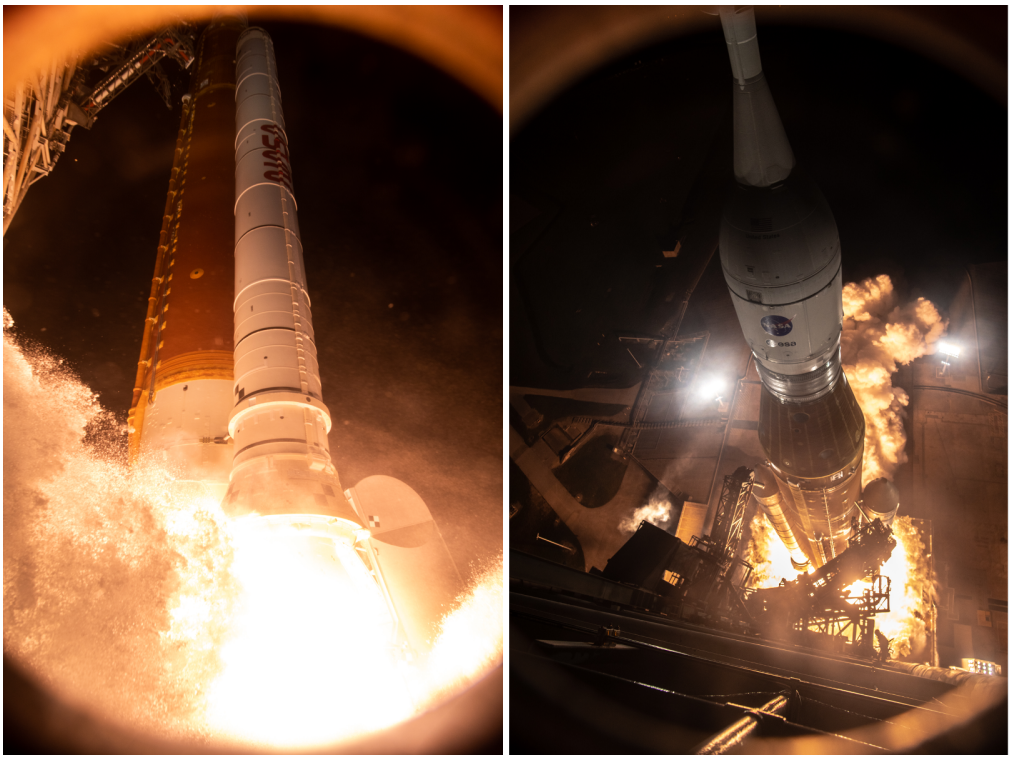

Fig. 1 Images from the November 16, 2023 Artemis I SLS launch, taken from Ref. [1].

One aspect of the launch vehicle is its use of solid rocket boosters (SRBs) to augment the liftoff and initial ascent mission stages. Inherited from the Space Shuttle Program, these boosters provide nearly 80% of the vehicle thrust at liftoff. Once their solid fuel is nearly spent, the boosters are jettisoned from the core stage, which then continues its ascent as the boosters fall into the ocean below. This booster separation event is aerodynamically complex: several engine plumes interact, including those of the core stage engines and the separation motors that propel the boosters away from the core stage. The three bodies move in close proximity, independently of one another, at supersonic speeds. A great deal of effort goes into ensuring, to a high degree of confidence, that the boosters and core stage will not recontact during the separation event. The aerodynamic aspect of this prediction effort is detailed in Ref. [2].

However much effort went into the Artemis I launch vehicle design and analysis, it was not until after the November 2022 launch that those methods could be validated with real flight data. This paper details these post-flight analyses

of the booster separation event. In particular, integrated separation trajectory simulations and computational fluid dynamics plume modeling are shown to agree with Artemis I flight data.

II. Preflight Trajectory Simulations

CLVTOPS [3] is a multibody dynamics simulation tool that was developed specifically to model high-fidelity clearances during various flight events, such as liftoff and booster separation. CLVTOPS serves as a multifunctional wrapper around the TREETOPS [4] dynamics engine and provides capabilities such as the ability to run Monte Carlo analyses with hundreds of dispersed variables, a robust post-processing capability, and generation of output files compatible with the NASA-developed Tree3D [5] visualization software package.

Preflight booster separation analyses for Artemis I were conducted using CLVTOPS and included several day-of-launch specific inputs to best represent the expected vehicle configuration and trajectory on launch day. Examples of the most influential models are the SRB flight day performance prediction, SRB pyro timing model, SLS guidance, navigation, and control (GNC) model, SLS integrated vehicle mass properties, SRB propellant mean bulk temperature (PMBT), and booster separation aerodynamics.

PMBT of the solid rocket motor propellant of both the SRBs and Booster Separation Motors (BSMs) is a major performance driver and is used as a key input parameter to scale the thrust and burn rate. The PMBTs of the boosters impact the vehicle states, such as dynamic pressure and Mach number at booster separation, essentially setting the initial conditions for the separation event. Hot booster PMBTs cause an increase in burn rate, resulting in earlier separation, which tends to cause lower-altitude separations with higher dynamic pressure and, therefore, larger aerodynamic loads. Due to the earlier separation, hot PMBTs are also correlated with higher core propellants mass, resulting in a lower core axial acceleration at separation. The PMBTs of the BSMs then largely govern the vehicle dynamics after separation has occurred. Hot BSMs separate the boosters from the core more quickly, generally allowing for more clearance of the external components of the SRBs and core. However, this increased lateral acceleration also tends to reduce clearances in the forward core-booster attach hardware. Thus, the hottest and coldest BSM PMBTs drive worst-case clearances for different areas of the hardware.

In order to bound expected vehicle performance across the entire year, drive worst-case clearances across all launch months, and to obviate the need for a more exhaustive set of simulation cases, four booster separation cases (Figure 2) were designed that encompassed all possible combinations of SRB and booster BSM PMBTs across the entire year of launch windows.

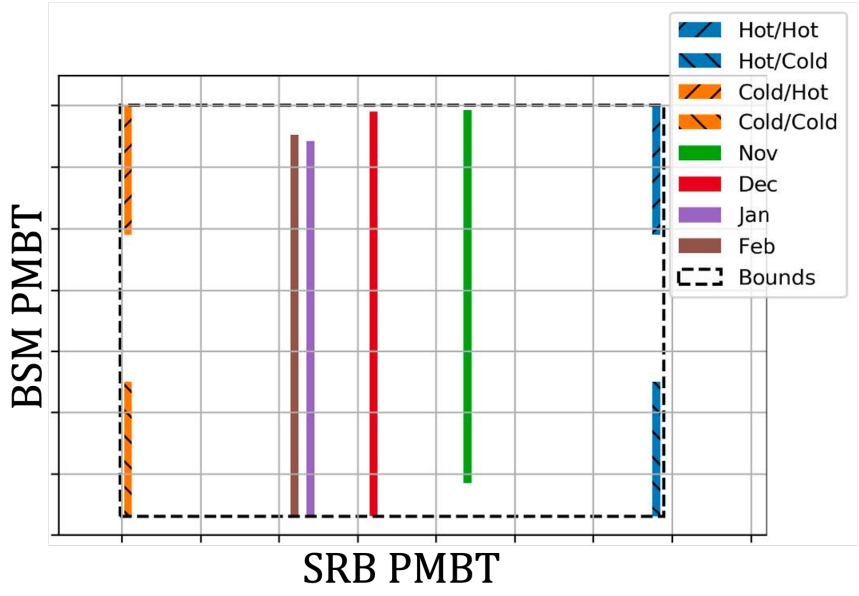

Fig. 2 Artemis I booster separation analysis PMBT design box.

Other than PMBT, the model input that varied per specific launch day was the GNC input that guided the vehicle

trajectory. Artemis I booster separation analysis showed that booster separation clearance results had low sensitivity to launch day differences based on these GNC inputs, so PMBT was used as the overarching design input to drive worst-case clearances. The other inputs noted above such as mass properties, separation aerodynamics, and pyro timing do not vary with vehicle configuration/launch day.

Four primary clearance metrics were used for booster separation analysis to determine the amount of margin with respect to booster-to-core recontacts that is predicted for the Artemis I vehicle:

1) minimum forward attach ball/socket clearance when the ball passes the socket exit plane;
2) minimum clearance between an aft attach strut to the opposite body (generally the aft end of the core-to-booster-side diagonal strut stub);
3) minimum macro clearance between a booster and the core stage when the nose of the booster crosses the exit plane of the core stage engines axially; and
4) forward attach TPS clearance, defined by the clearance between the TPS-coated crossover fairing geometry on the core side and the TPS-coated "outer" forward attach hardware on the booster side.

The four plots in Figure 3 show the worst-case clearances for each of these four metrics and the plot title describes the specific PMBT combination that resulted in this clearance result. Note that even though these are "worst-case" clearances, each plot shows that the clearance continuously increases after separation, indicating no recontacts were expected.

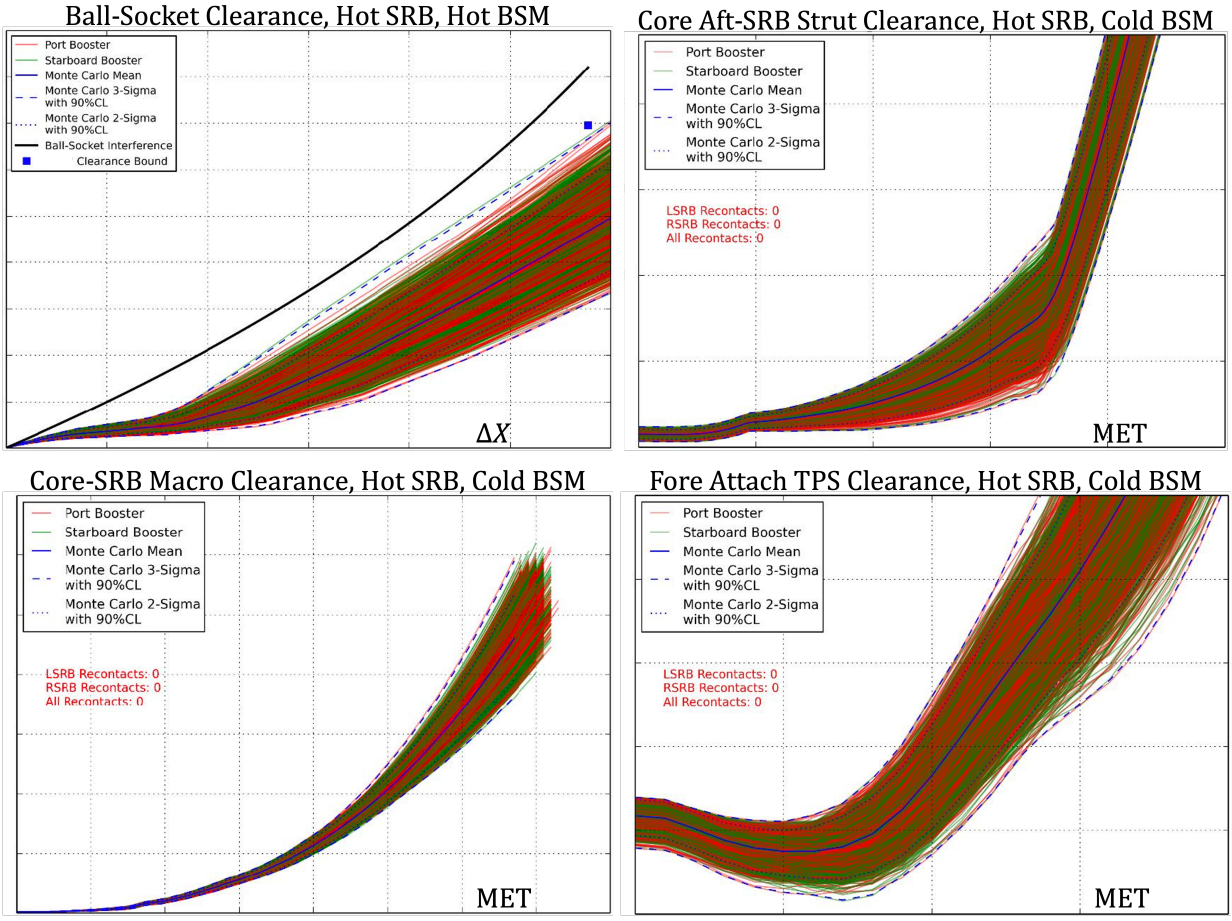

Fig. 3 Plots of dispersed trajectory sets yielding bounded estimates of critical core-booster clearances for Artemis I launch windows that together account for all expected extremes within the launch year. Note that one plot is a function of axial booster separation ΔX and the others are functions of mission-elapsed time (MET).

The Artemis I booster separation analysis showed positive clearances between the boosters and core stage; the use of bounding PMBTs as well as low sensitivity of clearances to variations in launch date indicate that these positive

results should hold for all potential launch periods.

III. Post-Flight Analyses

Prior to the moment that the boosters separate from the core stage, all flight instrumentation on the boosters is sent through the attach hardware to data acquisition units on the core stage, and core stage hardware is also responsible for transmitting that data to the ground. As a result, once separation occurs, there are no data from the boosters themselves. This means that no surface pressures, combustion chamber pressures, heat fluxes, acceleration data, etc. are available to help validate predictions about the trajectory and flow fields during booster separation. However, this did not disable all efforts to validate the vehicle predictions with flight data. Two analyses were performed on the Artemis I booster separation event: a simplified trajectory comparison and a core stage pressure sensor investigation. This section presents the details of and the findings from both of these assessments.

A. Trajectory Comparisons

The night launch of the Artemis I mission limited ground-based visibility during booster separation. However, due to the light emitted from the booster separation motors and the core stage engines, a small amount of points were illuminated for enough of the separation event, from the perspective of on-board cameras, that a simple trajectory reconstruction could occur. Two examples of this are presented in Figure 4.

(a) RSRB **(b) LSRB**

Fig. 4 Images captured by core stage cameras of the Artemis I booster separation event. Light from the engines illuminates a small number of photogrammetry points (e.g., black strips) on both boosters [photo: NASA].

Given the known preseparation locations of the photogrammetry points on the boosters, frame-by-frame image analysis was performed on these onboard videos, which resulted in position estimates of these surface markings as functions of time. The procedure of performing this image analysis is out of the scope of this paper; readers are directed to Ref. [6] for an introduction to the governing principles and to Ref. [7] for a summary of the photogrammetry effort as it pertains to the SLS.

Once the positions of these photogrammetry points are estimated as functions of time, they can be reconciled into booster nose position estimates. This procedure is straightforward as long as it is assumed that the boosters remain rigid bodies during the separation event. Given any three booster surface point positions 1, 2, 3 relative to a global reference point 0, $\vec{p}_{01,02,03}$, a local coordinate system $\hat{e}$ can be defined based on the vectors connecting these points and their cross product:

$$\begin{aligned} \hat{e}_1 &= \vec{p}_{12}\,|\vec{p}_{12}|^{-1} \\ \hat{e}_2 &= \vec{p}_{13}\,|\vec{p}_{13}|^{-1} \\ \hat{e}_3 &= \hat{e}_1 \times \hat{e}_2 \end{aligned} \tag{1}$$

where the $|\cdot|$ brackets denote a vector magnitude and the $\times$ operator denotes a vector cross product. The position vector between this local axis system locus (in this example point 01) and any other point on the rigid body, $\vec{p}_{1n}$, is constant

as long as the body remains rigid. In the local coordinate system, this is represented as

$$\vec{p}_{1n} = \vec{p}_{0n} - \vec{p}_{01} \tag{2}$$

$$= u\hat{e}_1 + v\hat{e}_2 + w\hat{e}_3 \tag{3}$$

where Equation 2 can be computed once with preseparation, known booster position measurements and Equation 3 can be computed at subsequent post-separation instances where $\vec{p}_{01}$ is measured and u, v, w have not changed. In this way, given the photogrammetry point positional estimates, the booster nose position can be computed at any time at which at least three photogrammetry points are visible.

Figure 5 presents booster nose positions as functions of both mission-elapsed time (MET) and axial preseparation relative distance, ΔX. Nose positions as computed from a trajectory simulation with all nominal conditions are plotted as solid lines; nose positions as computed from flight data are plotted as points. The large gaps between points are where fewer than three photogrammetry points were visible at any given video frame.

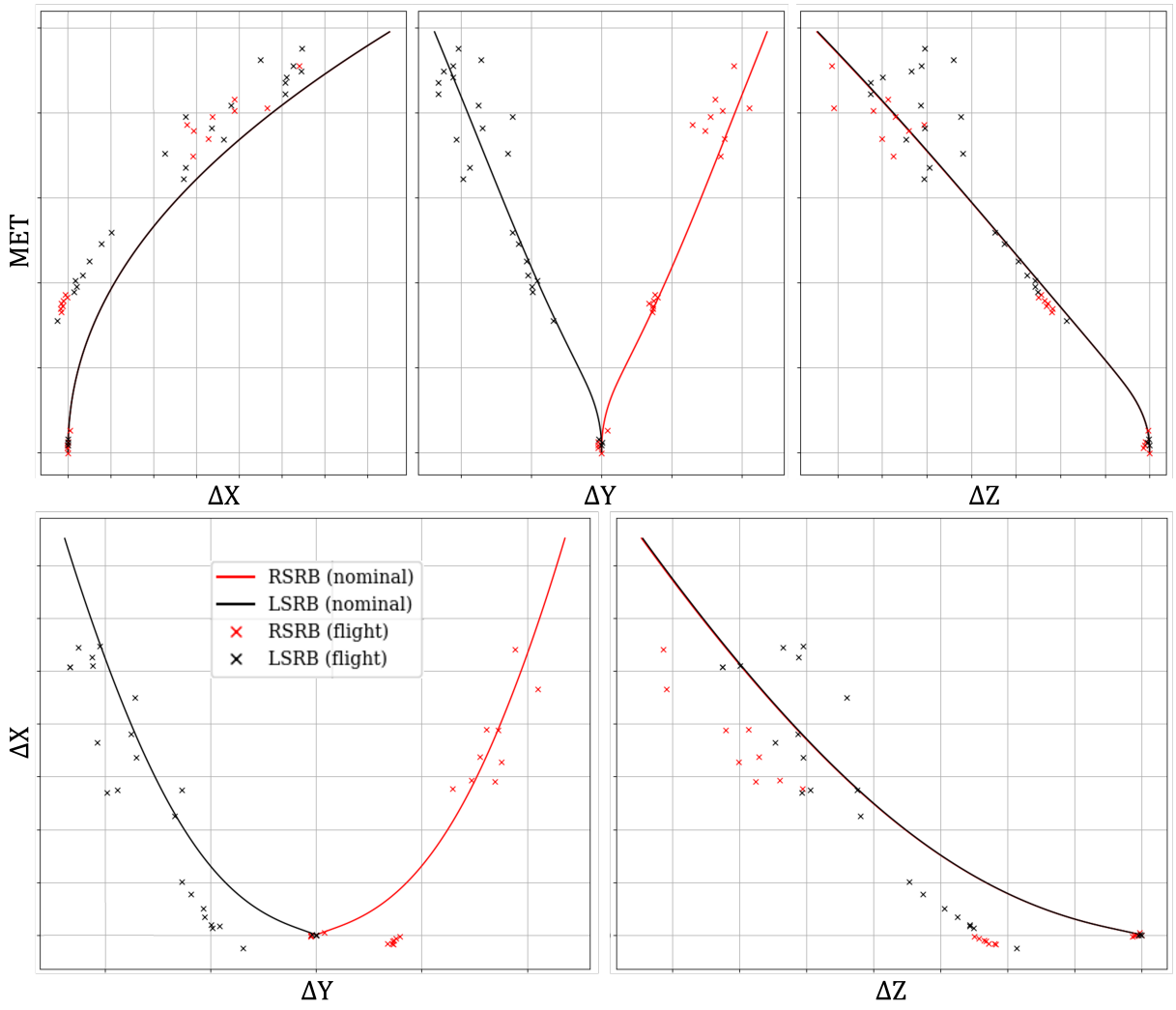

Fig. 5 Booster nose positions plotted as functions of mission-elapsed time (top) and as functions of the axial separation distance ΔX (bottom), as computed from both trajectory simulations and Artemis I flight data. Where both lines are not visible, the black line directly overlaps the red line due to the simulated symmetry of the booster physics with no uncertainties applied.

Given the uncertainties in both the flight data and the trajectory simulation, the general agreement between the trajectory simulations and the flight data estimates is encouraging. It was understood during their creation that photogrammetry estimates after the first moments of separation were less accurate; this is reflected in the increased dispersion of

flight data at higher separation distances. The jagged trends drawn by the flight data are clearly measurement errors and not physically infeasible booster dynamics. Where the photogrammetry estimates are most confident, there is a strong agreement between the two data sources. Where the photogrammetry estimates are less confident, the nominal separation trajectory traces a path directly through the cloud of point estimates.

B. Fluid Dynamics Simulations

Despite the absence of flight data from the boosters post-separation, some of the core stage pressure sensors are still active in this portion of the flight. Fortunately, two of the approximately two dozen core stage pressure sensors are significantly impacted by the exhaust from the Booster Separation Motors (BSMs), and as a result there is a small amount of flight data to help validate the flow fields predicted by CFD.

New FUN3D simulations, following the same techniques used for Artemis II booster separation described in Ref. [8], were run at every 0.2 ft of axial SRB translation. Due to the limited photogrammetry in the first second after booster separation, only a crude SRB trajectory could be assembled for this study. The sources for this small run matrix are:

- the Artemis I Best Estimated Trajectory (BET), for atmospheric conditions (dynamic pressure, temperature);
- Artemis I preflight booster separation simulations, for mean SRB positions and angles; and
- Artemis II booster separation simulations, for thrust profiles.

These FUN3D simulations used 130.9 s MET as the time of separation, but the best current estimate is 130.818 s MET. The FUN3D results should be shifted slightly to the left for a more accurate comparison.

Figure 6 shows the comparison between flight data and the post-flight FUN3D simulations for the `AD-P012` sensor, which is the only sensor on the left side of the core stage that presented evidence of BSM plume impingement. Figure 7 does the same for the `IV-AT-P003-C` sensor, which is the only sensor on the right side of the core stage observed to experience BSM plumes. Despite the differences between flight and simulation data, these results have been interpreted as a positive outcome. Several factors prevent the expectation of a close match:

- the simulations use only a very rough approximation of SRB trajectories, and the point pressures are highly sensitive to SRB position and orientation;
- the developmental flight instrumentation (DFI) is not well-calibrated at this point in flight;
- the point pressures would also be sensitive to the installation orientation of the BSMs such that even small angle differences within the design tolerances are important.

A concrete positive result is that of the pressure sensors on the core stage formatted to collect data during this phase of flight, only these two measured a significant pressure rise during booster separation, and only these two had a simulated pressure rise of significance in the FUN3D simulations.

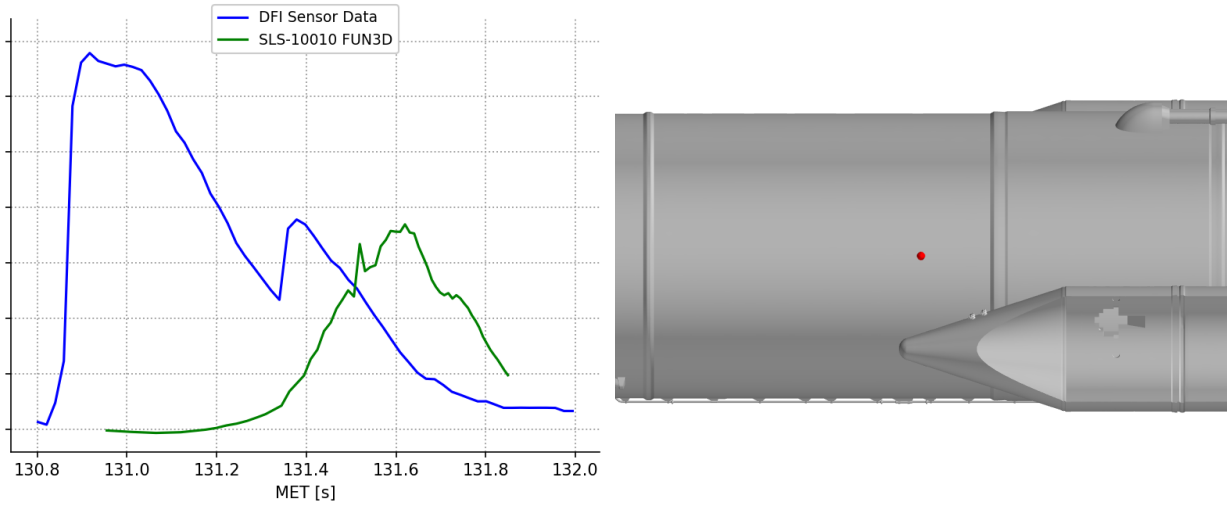

(a) Time history of C_P for sensor `AD-P012`

(b) Location of sensor `AD-P012`

Fig. 6 Booster separation C_P history for sensor `AD-P012` on the left side of the core stage.

Of note in the flight data for both sensors is the prominent two-peak nature. To explain this result, Figure 8 shows a

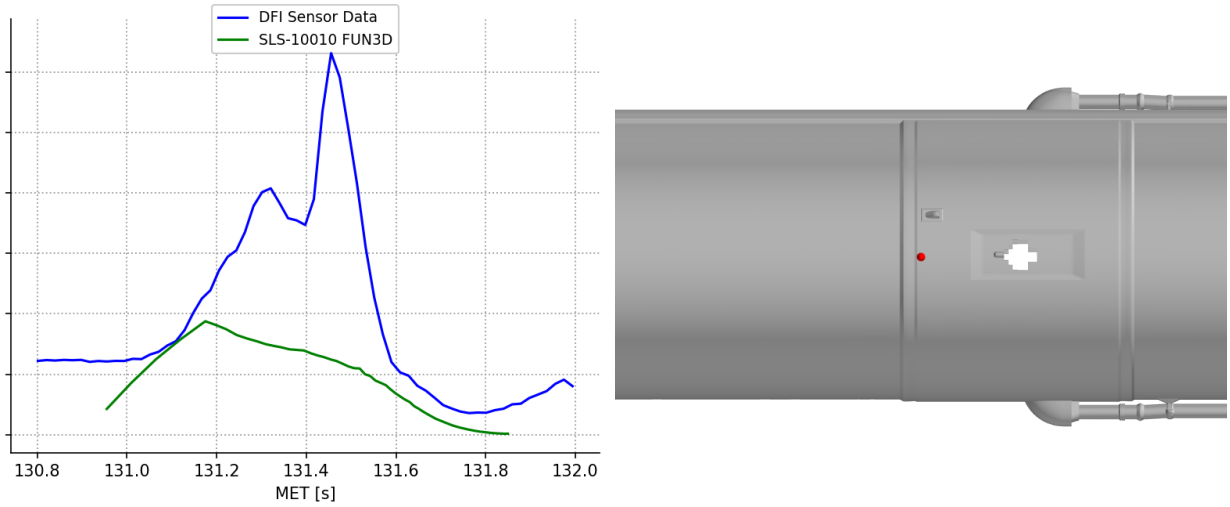

(a) Time history of C_P for sensor `IV-AT-P003-C` **(b) Location of sensor `IV-AT-P003-C`**

Fig. 7 Booster separation C_P history for `IV-AT-P003-C` sensor on the right side of the core stage.

close-in look at the core stage surface pressures around `IV-AT-P003-C` for a FUN3D simulation with a small amount of axial SRB translation. The plume impingement on the sensor location is apparent. The structure of this plume indicates that the pressure tap was indeed impinged upon, directly, by the booster separation motors. The fact that each separation motor is in fact four motors placed close to one another explains the two-peak nature of Figures 6 and 7: the sensor experienced plume impingement from more than one of the neighboring separation motors within a short period of time. Furthermore, Figure 8 shows that the peak C_P values in the impingement region are near the same magnitude as the flight data, assuming a near-direct hit did indeed occur.

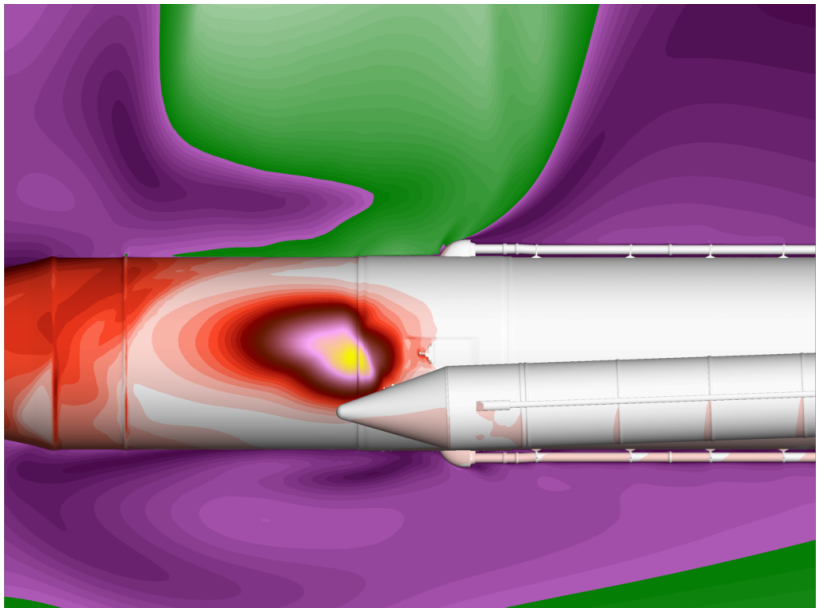

Fig. 8 Surface C_P of BSM plume impingement on the core stage with a low ΔX.

The timing of the `AD-P012` pressure rise is the main unexplained difference, but the expectation is that a precise SRB trajectory reconstruction would improve the comparison there. It is also possible that the precise timing of when booster separation occurred could be significant in understanding this rapid pressure rise.

IV. Conclusion

The successful Artemis I booster separation event has been studied as a basis for validation of the design procedures that enabled the SLS vehicle. Prior to launch, many sets of Monte Carlo trajectory simulations integrated a spectrum of physics models to anticipate a likely separation path envelope. This envelope was used to assert, with a high degree of confidence, that the three vehicle components would not contact one another after the initial separation event.

These trajectory estimates were validated at an integrated level with flight data booster position reconstructions. Photogrammetry markers on the boosters enabled such reconstructions to occur, though the uncertainty in these reconstructions increased as the boosters moved further from the core stage. Despite this high uncertainty, the nominal separation trajectory was observed to trace the middle of the flight data cloud.

Fluid flow simulations along the estimated booster separation trajectory enabled a reconstruction of recorded surface pressure measurements. Although, due to flight hardware constraints, no flight data were recorded from the boosters after separation, two core stage pressure taps directly experienced the booster separation motor plumes. Comparison of these pressure tap records to the simulated core stage pressures yielded promising comparisons as well: that the modeled plumes only impinged on two tap locations, and that the flight data agreed with this assessment.

The encouraging results presented in this paper serve to validate the processes developed to model this extremely complicated launch event. It is important to remember, however, that the flight data defines just one separation event out of many viable events. The inherent complexity of the system means that this one success does not indicate that less prudence is necessary for the next mission. Rather, the vehicle design infrastructure can now be further refined with confidence that, at an integrated level, the collective effort appears to adequately represent the most apparent system physics.

Acknowledgments

Appreciation is extended to H. Houlden (ViGYAN Inc.) and D. Chan (NASA LaRC) for their development of previous SLS booster separation databases. Thanks are given to D. Osborne (NASA MSFC), M. Cisse (NASA MSFC), and B. Nazeri (Bevilacqua Research Corporation) for their efforts in reconstructing the photogrammetry marker positions from flight videos.

References

[1] Kraft, R. H., "View the Best Images from NASA's Artemis I Mission," , 2022. URL `https://www.nasa.gov/humans-in-space/view-the-best-images-from-nasas-artemis-i-mission/`.

[2] Lee, M., Dalle, D., Sanders, M., and Addona, C., "Development of Aerodynamic Loads Databases for the Space Launch System Booster Separation Event," *AIAA SCITECH 2024 Forum*, 2024.

[3] Burger, B. S., Addona, C., Diedrich, B., Harlin, W., McDonough, P., Muscha, Z., Sells, H., and Tyler, D., "Space Launch System Liftoff and Separation Dynamics Analysis Tool Chain," *AIAA Scitech 2021 Forum*, 2021, p. 0822.

[4] "TREETOPS," , MFS-33566-1. URL `https://software.nasa.gov/software/MFS-33566-1`.

[5] "Tree3D Dynamics Visualization Tool," , MFS-34076-1. URL `https://software.nasa.gov/software/MFS-34076-1`.

[6] Schenk, T., "Introduction to Photogrammetry," *The Ohio State University*, 2005.

[7] Ali, R., Burger, B., Addona, C., and Mcdonough, P., "Post Flight Clearance Analysis by Photogrammetric Reconstruction," *Aerospace Control and Guidance Systems Committee Meeting# 127*, 2021.

[8] Meeroff, J. G., Dalle, D. J., Rogers, S. E., Burkhead, A. C., Schauerhamer, D. G., and Diaz, J. F., "Advances in Space Launch System Booster Separation CFD," *AIAA SCITECH 2023 Forum*, 2003. https://doi.org/10.2514/6.2023-0238, aIAA Paper 2023-0238.